

BACHELOR

Electric field profiling inside an inverse cavity using MCRS

Clevis, Roy H.J.

Award date:
2019

[Link to publication](#)

Disclaimer

This document contains a student thesis (bachelor's or master's), as authored by a student at Eindhoven University of Technology. Student theses are made available in the TU/e repository upon obtaining the required degree. The grade received is not published on the document as presented in the repository. The required complexity or quality of research of student theses may vary by program, and the required minimum study period may vary in duration.

General rights

Copyright and moral rights for the publications made accessible in the public portal are retained by the authors and/or other copyright owners and it is a condition of accessing publications that users recognise and abide by the legal requirements associated with these rights.

- Users may download and print one copy of any publication from the public portal for the purpose of private study or research.
- You may not further distribute the material or use it for any profit-making activity or commercial gain

EINDHOVEN UNIVERSITY OF TECHNOLOGY

BACHELOR FINAL PROJECT

ELECTRIC FIELD PROFILING INSIDE AN INVERSE CAVITY USING MCRS

ELEMENTARY PROCESSES IN GAS DISCHARGES

WRITTEN BY

ROY CLEVIS 1015431

SUPERVISORS
PATRICK MEIJAARD
JOB BECKERS

DATE JULY 1, 2019



Abstract

Microwave cavity resonance spectroscopy has been used as a means to determine the electric field pattern of five different modes inside an inverse cylindrical cavity. The pattern is obtained by positioning a bead of barium titanate(IV) inside the cavity and measuring the frequency shift, which relates directly to the square of the electric field at the position of the bead. The calculated and measured patterns are compared to each other and found to be similar with the exception of a few intensities differences. Two possible methods of improvement have been described and executed, one with a different pattern. This methods did increase the accuracy of the electric field pattern. Two different antennas were compared and it was found that the quality factor of the mode is also dependent of the design of the antenna.

Contents

List of Figures	3
List of Tables	4
1 Introduction	5
2 Microwave cavity resonance spectroscopy	6
2.1 Electromagnetic fields inside a cylindrical cavity	6
2.2 TE and TM modes	7
2.3 Perturbation by dielectric material	7
2.4 Quality factor	8
2.5 Calculated electric field patterns	10
2.6 Plasma diagnostics using MCRS	10
3 Experimental setup	12
3.1 Setup	12
3.1.1 Stepper motor movement	13
3.1.2 MATLAB script	14
3.1.3 Cavity design and Bead pattern	15
3.2 Frequencies	15
3.2.1 Fitting	16
3.3 One side movement	17
3.4 Improvement signal	18
4 Results and Discussion	20
4.1 TM010	20
4.2 TM011	21
4.3 TM013	21
4.4 TE213	22
4.5 TM014	22
4.6 One sided movement	23
4.7 Improvement antenna	24
4.7.1 Antenna 2	24
4.7.2 Antenna 3	25
4.8 Discussion	26
5 Conclusion	27
Bibliography	29
A Temperature sensor calibration	30
B Frequency table	31

C	Matlab scripts	32
C.1	Main script	32
C.2	Script for making the connection to the measuring devices	33
C.3	Script for making a single MCRS measurement	34

List of Figures

2.1	Cylindrical coordinates	6
2.2	A resonance peak of an arbitrary mode. Image taken from [6].	9
2.3	Contour plots of the squared electric field for five different modes of the cylindrical cavity. The first three contour plots share the same legend.	10
3.1	Schematic image of the used setup	12
3.2	Photo of the used antenna.	14
3.3	Photo of the cylindrical cavity.	14
3.4	Linear relation between position and the ADC voltage measured.	14
3.5	The pattern that the bead will follow during the measurement of one slit, each circle represents the position of the bead during a single MCRS measurement.	15
3.6	Measured response of the cavity for the frequency range from 2GHz to 6GHz. The reflectivity is measured in decibels and the frequency in Hertz. This image is made using the antenna from figure 3.2.	16
3.7	Cavity response for the 5 different modes.	17
3.8	The pattern that the bead will follow during the new measurements of one slit, each circle represents the position of the bead during a single MCRS measurement.	17
3.9	Antennas 2 and 3	18
3.10	Cavity response for antenna 2 for the two modes.	18
3.11	Cavity response for antenna 3 for the two modes.	19
4.1	TM010	20
4.2	TM011	21
4.3	TM013	21
4.4	TE213	22
4.5	TM014	22
4.6	Electric field pattern of the third slit for the five different modes, using the measurement pattern as describe in 3.3. The graphs are not to scale.	23
4.7	TM010 antenna 2	24
4.8	TM011 antenna 2	24
4.9	TM010 antenna 3	25
4.10	TM011 antenna 3	25
A.1	Calibration of the used temperature sensor, done by I. Bolk.	30

List of Tables

2.1	Overview of the electric and magnetic field equations	8
B.1	Frequencies of each mode as calculated using equation 2.5	31

Chapter 1

Introduction

In this chapter a brief introduction is given to the topic of this study. Also the contents of each chapter are shortly described.

Plasma is the fundamental fourth aggregate state of matter, next to the ordinary states of liquid, solid and gas. Plasmas are ionized gasses [2], plasmas can be formed for example in high temperatures and by using strong electrical field. A large portion of the universe is made up of matter in a plasma state, all stars for example are made up of plasma [4]. Typical plasmas are neutral as a whole, since the negative electrons are separated from a now ionized atom or molecule, this is called quasi-neutrality since there are charges present in the plasma [11].

Plasmas have a variety of properties, free electron density, temperature and pressure are a few of them. The free electron density, the amount of electrons that are not bound to an atom per a unit of volume, is a property that is difficult to measure without affecting the plasma [8].

Different diagnostics that can measure the electron density are Langmuir probes, optical emission spectroscopy, Thomson scattering, microwave interferometry and microwave cavity resonance spectroscopy. Non of these methods can measure the electron density in spatial and temporal dimensions at the same time [6].

This study uses an inverse cylindrical cavity. An ordinary cylindrical cavity creates plasma by applying a RF voltage to the top or bottom of the cavity. In an inverse cylindrical cavity this RF voltage is applied to the curved wall of the cylinder.

Microwave cavity resonance spectroscopy (MCRS) is used in this study. MCRS is a diagnostic to measure the average free electron density if the electric field pattern is unknown and in the case where the electric field pattern is known it can be used to measure the free electron spatial distribution. A standing electromagnetic wave will be excited inside the cavity, the frequency of this wave is dependent on the distribution of particles and their relative permittivity throughout the cavity. One of the advantages of MCRS is that it is a non-intrusive method. Using the same technique on an empty cavity (no plasma) the electric field pattern can be determined with the use of a small perturbation in the form of a Barium Titanate(IV) bead. This study focusses on obtaining the electric field patterns inside a cylindrical inverse cavity. This gives the following research question: what does the electric field profile look like inside an inverse cylindrical cavity, for different resonance frequencies?

In chapter 2 a theoretical basis will be given on electric fields inside a cylindrical cavity and the theoretical prediction of the field will be given. Following in chapter 3 the experimental setup is described and the process of measuring is described, also different improvements are explained. In chapter 4 the result of the measurements are shown and described, also a discussion of the results is given. Finishing with chapter 5 the research question is answered using the results and taking into account the discussion.

Chapter 2

Microwave cavity resonance spectroscopy

In this chapter the theoretical background of the research is given. It will start with a general overview of electric fields inside a cavity and continue with how a small perturbation can be used as a way to determine the electric field pattern inside a cavity. Different field patterns are calculated and visualised. Lastly the link to plasma diagnostics is made.

2.1 Electromagnetic fields inside a cylindrical cavity

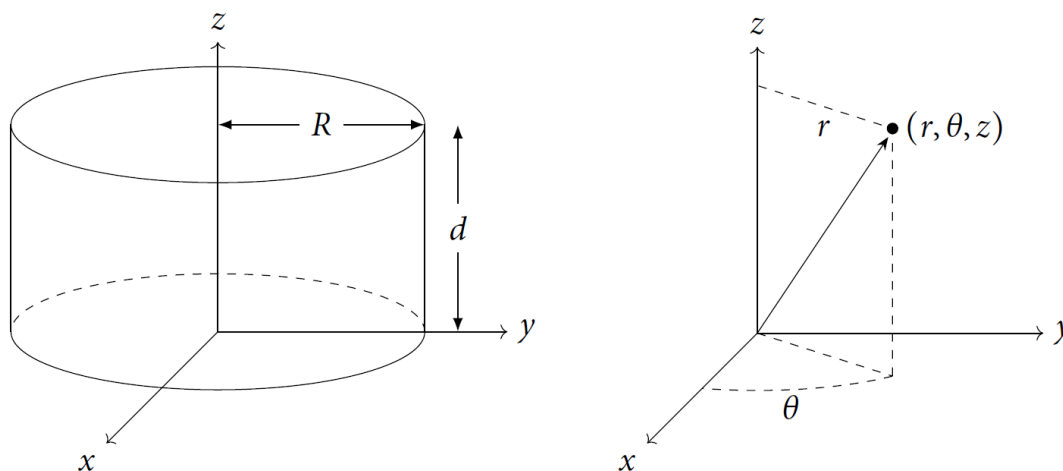


Figure 2.1: On the left side is a cylinder in a cartesian coordinate system, with a radius R and height d . On the right side is a representation of cylindrical coordinates (r, θ, z) . Image taken from PhD thesis Ferdi van de Wetering [6].

Electromagnetic waves inside a closed cavity do not propagate, but can form standing waves. A cylinder positioned around the z -axis from $z = 0$ to $z = d$ and a radius R , see figure 2.1, is taken. The material of the walls of the cylinder is assumed to be an ideal conductor, the conductivity is equal to infinity. For an ideal conductive material the electric field inside the material is equal to 0 [7], this is because the free electrons in the material immediately cancel out any existing field or changing field. The same holds for the magnetic field, inside the walls of the cavity the magnetic field equals 0 [5]. Using the Maxwell equations [7]

$$\nabla \cdot \mathbf{E} = \frac{\rho}{\varepsilon_0}, \quad \nabla \times \mathbf{E} = -\frac{\partial \mathbf{B}}{\partial t}, \quad (2.1)$$

$$\nabla \cdot \mathbf{B} = 0, \quad \nabla \times \mathbf{B} = \mu_0 \left(\mathbf{J} + \varepsilon_0 \frac{\partial \mathbf{E}}{\partial t} \right), \quad (2.2)$$

where \mathbf{E} is the electric field vector, \mathbf{B} is the magnetic field vector and \mathbf{J} is the current density vector, ρ is the charge density, ε_0 is the permittivity of the vacuum and μ_0 is the permeability of the vacuum, it is possible to obtain the boundary conditions for the surfaces of the cavity. The boundary conditions are given by the following equations [7]

$$\hat{\mathbf{n}} \cdot \mathbf{E} = \frac{\sigma}{\varepsilon} \quad (2.3)$$

and

$$\hat{\mathbf{n}} \times \mathbf{B} = \mu \cdot \mathbf{K}, \quad (2.4)$$

with $\hat{\mathbf{n}}$ the normal vector of the cavity wall pointing inside, σ the surface charge density and \mathbf{K} the displacement current. In words these conditions mean that the change of the component perpendicular to the surface of the electric field vector is equal to the surface charge over the permittivity, subsequently the change in the parallel component is equal to zero, meaning that the electric field at the surface only has a perpendicular component since the electric field inside the walls is 0. For the magnetic field, the component perpendicular to the surface of the magnetic field is equal to 0 because the magnetic field inside the wall is 0. The parallel component is equal to the permeability times the surface current.

2.2 TE and TM modes

Inside a cavity there are two main configurations, also called modes, of standing waves, transverse electric (TE) and transverse magnetic (TM). Transverse electric means that the electric field is perpendicular to the propagation direction in this case the central axis of a cylinder, so $E_z = 0$. Similar to TE the transverse magnetic mode means the magnetic field is perpendicular to the central axis, $B_z = 0$. Solving the Maxwell equations with the boundary conditions given in equations 2.3 and 2.4 and for the two different modes gives the equations in table 2.1 [6].

Each mode is defined as TM_{mnp} for TM modes and TE_{mnp} for TE modes, with indices m, n and p integer numbers, generally $m \geq 0, n \geq 1$ and $p \geq 0$. Each mode has its own frequency determined by

$$f_0 = \frac{1}{2\pi} \sqrt{\frac{k_r^2 + k_z^2}{\varepsilon\mu}}. \quad (2.5)$$

Roughly speaking the value for m is the amount of nodes in the azimuthal direction, the n for the radial direction and the p for the z direction.

2.3 Perturbation by dielectric material

The frequency of the electric field is dependent on the material present inside the cavity, when putting a dielectric material inside the cavity the frequency changes to ω_p . The shift is dependent on the position of the dielectric and the electric field at that position. Also the value of the permittivity of the dielectric plays a role. The frequency shift due to the presence of a small dielectric particle with respect to the frequency of the electric field in vacuum, ω_{vac} , is given by [6]

Table 2.1: Overview of the electric and magnetic field equations for the two different modes TM and TE. With $J_m(x)$ the so called Bessel functions of the first kind and $J'_m(x)$ its derivative with respect to x . x_{mn} and x'_{mn} are the n^{th} zero of respectively $J_m(x)$ and $J'_m(x)$, for $x > 0$.

	TM	TE
E_r	$-E_0 \frac{k_z}{k_r} J'_m(k_r r) \cos(m\theta) \sin(k_z z)$	$-imE_0 \frac{J_m(k_r r)}{k_r} \sin(m\theta) \sin(k_z z)$
E_θ	$mE_0 \frac{k_z}{k_r} \frac{J_m(k_r r)}{k_r r} \sin(m\theta) \sin(k_z z)$	$-iE_0 J'_m(k_r r) \cos(m\theta) \sin(k_z z)$
E_z	$E_0 J_m(k_r r) \cos(m\theta) \cos(k_z z)$	0
B_r	$imB_0 J_m(k_r r) \sin(m\theta) \cos(k_z z)$	$B_0 \frac{k_z}{k_r} J'_m(k_r r) \cos(m\theta) \cos(k_z z)$
B_θ	$iB_0 J'_m(k_r r) \cos(m\theta) \cos(k_z z)$	$-mB_0 \frac{k_z}{k_r} \frac{J_m(k_r r)}{k_r r} \sin(m\theta) \cos(k_z z)$
B_z	0	$B_0 J_m(k_r r) \cos(m\theta) \sin(k_z z)$
k_r	$\frac{x_{mn}}{R}$	$\frac{x'_{mn}}{R}$
k_z	$\frac{p\pi}{d}$	$\frac{p\pi}{d}$
ω_0	$\sqrt{\frac{k_r^2 + k_z^2}{\epsilon\mu}}$	$\sqrt{\frac{k_r^2 + k_z^2}{\epsilon\mu}}$

$$\frac{\omega_p - \omega_{vac}}{\omega_{vac}} = -\frac{\iiint_{cav} \Delta\epsilon E^2 d^3\mathbf{x}}{2\epsilon_0 \iiint_{cav} E^2 d^3\mathbf{x}}. \quad (2.6)$$

Since $\Delta\epsilon = \epsilon_0 \Delta\epsilon_r = \epsilon_0(\epsilon_r - \epsilon_{r,air})$, $\epsilon_{r,air} = 1.00058986 \approx 1$ [1] and since the difference in permittivity outside the dielectric particle is equal to 0 this changes to

$$\frac{\omega_{vac} - \omega_p}{\omega_{vac}} = \frac{\epsilon_r - 1}{2} \frac{\iiint_{diel} E^2(\mathbf{x}) d^3\mathbf{x}}{\iiint_{cav} E^2(\mathbf{x}) d^3\mathbf{x}}. \quad (2.7)$$

Assuming that the size of the particle is sufficiently small so that the electric field is constant across the volume of the particle V_{diel}

$$\frac{\omega_{vac} - \omega_p}{\omega_{vac}} = \frac{\epsilon_r - 1}{2} \frac{V_{diel} E^2(\mathbf{x}_{diel})}{\iiint_{cav} E^2(\mathbf{x}) d^3\mathbf{x}}. \quad (2.8)$$

Since all variables are constant except for the electric field squared this can be written in the following form

$$E^2(\mathbf{x}_{diel}) \propto \frac{\omega_{vac} - \omega_p}{\omega_{vac}}. \quad (2.9)$$

Therefore measuring the frequency shift as a result of a small perturbation for a position \mathbf{x} will give the relative strength of the electric field at that position.

2.4 Quality factor

Up until this point it is assumed that the material of the cavity is an ideal conductor, infinite conductivity, however this is not the case. If the cavity were ideal the resonance peak would be looking the same as a

delta peak [10], for a non ideal cavity this is a broader peak see figure 2.2. The cavity has a so called quality factor (Q). The Q -factor is related to the energy loss in the cavity according to the following equation

$$Q = \omega_0 \frac{\text{averaged energy stored}}{\text{energy lost per second}}. \quad (2.10)$$

When the signal for the electric field is shut off the energy stored inside the cavity will act like a damped oscillator, and it will damp like [6]

$$\mathcal{E}(t) = \frac{\mathcal{E}_0}{2} \exp\left(-\frac{\omega_0}{Q} t\right). \quad (2.11)$$

The time scale on which the dampening happens is

$$\tau = \frac{2Q}{\omega_0}. \quad (2.12)$$

τ is also called the response time of the cavity. This means that any change in resonance frequency can be measured with a temporal resolution of τ . Therefore it is essential to know the Q -factor for each mode when measurements are done in the same order as this time scale.

The quality factor can be determined by measuring a resonance peak and its full width half maximum (FWHM) from the relation

$$Q = \frac{f}{\Delta f} = \frac{\omega_0}{\Gamma}, \quad (2.13)$$

with f the resonance frequency, Δf the FWHM in ordinary frequency, ω_0 the resonance angular frequency and Γ the FWHM in angular frequency. For high Q -factors the energy loss is small, making the cavity more ideal [3].

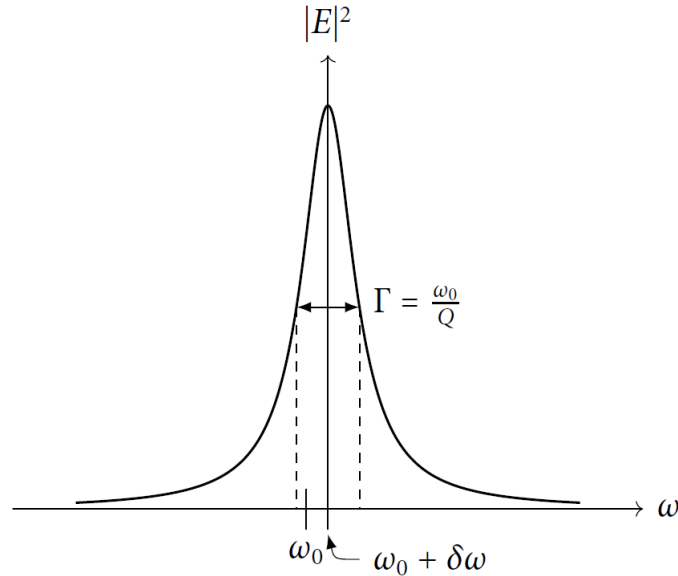


Figure 2.2: A resonance peak of an arbitrary mode. Image taken from [6].

2.5 Calculated electric field patterns

The dimensions of the cavity are known, therefore the theoretical pattern of the electric field can be calculated using the equations given in section 2.2. The radius of the cavity is $R = 52.525\text{mm}$ and the height is $d = 118.00\text{mm}$. With the use of Wolfram Mathematica 12 [12] and the equations the images in figure 2.3 are obtained for the square of the electric field as a function of r and z . The $\text{TM}01p$ modes, with p an arbitrary value, do not have an azimuthal dependency and can therefore easily be visualised using a contour plot, the $\text{TE}213$ does have an azimuthal dependency and is therefore plotted for different angles θ . The square of the electric field is plotted from $r = -R$ to $r = R$ on the horizontal axis and from $z = 0$ to $z = d$ on the vertical axis.

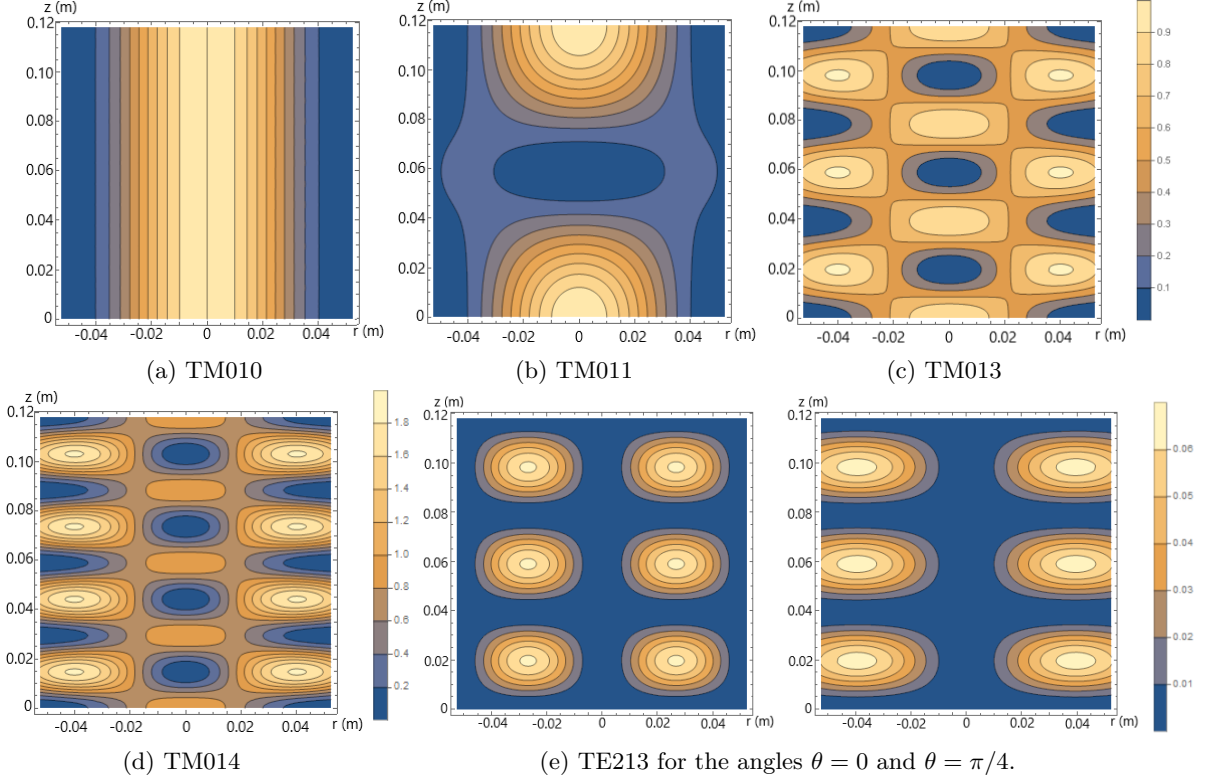


Figure 2.3: Contour plots of the squared electric field for five different modes of the cylindrical cavity. The first three contour plots share the same legend.

In section 3 will be explained how these images can be determined experimentally.

2.6 Plasma diagnostics using MCRS

MCRS can be used to determine free electron densities inside a plasma, since the presence of free electrons changes the permittivity ε . The same way the bead in section 2.3 changes the frequency the present electrons will change the frequency. The change in permittivity due to the presence of free electrons is given by [6]

$$\Delta\varepsilon = -\frac{n_e e^2}{m_e \omega_p^2}. \quad (2.14)$$

Substituting equation 2.14 into equation 2.6 gives the following equation for the spatial average of the free electron density

$$\bar{n}_e = \frac{2m_e \varepsilon_0 \omega_p^2}{e^2} \frac{\omega_p - \omega_{\text{vac}}}{\omega_{\text{vac}}}. \quad (2.15)$$

However the free electron density is not homogeneous distributed in all cases. When the spatial distribution is taken into account the spatial average of the free electron density changes to

$$\bar{n}_e \equiv \frac{\iiint_{\text{cav}} n_e(\mathbf{x}) E^2(\mathbf{x}) d^3\mathbf{x}}{\iiint_{\text{cav}} E^2(\mathbf{x}) d^3\mathbf{x}}. \quad (2.16)$$

The free electron density is weighted by the square of the electric field pattern of the resonance mode to get the average free electron density.

Chapter 3

Experimental setup

This chapter will describe the setup that is used to determine the electric field pattern. First the devices that are used will be described and the frequencies and corresponding modes that will be used to obtain the electric field patterns are chosen. Secondly two ways to improve the measurements are discussed.

3.1 Setup

As described in chapter 2 the distribution of the square of the electric field will be determined for different modes inside a specific cylindrical cavity. Below is a schematic image of the used setup.

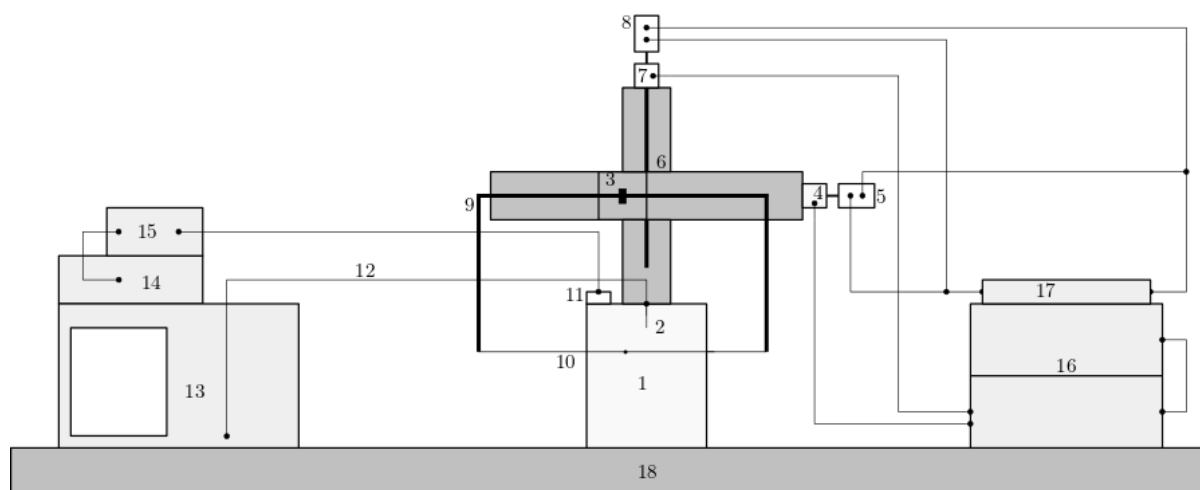


Figure 3.1: Schematic image of the used setup. 1) cavity 2) antenna 3) horizontal stage 4) horizontal stepper motor 5) horizontal resistor 6) vertical stage 7) vertical stepper motor 8) vertical resistor 9) frame holding the wire 10) wire with attached bead 11) temperature sensor 12) Silverline SLU18-SMNM-01.00M cable 13) network analyzer 14) digital multimeter 15) temperature sensor read-out 16) signal conditioning unit and practicum power unit 17) CaDPiPE board and RaspberryPi 18) optical table.

The cavity (1), see figure 3.3, with an antenna (2), see figure 3.2, is positioned in front of two stepper motors, nanotech ST4018L1804-KOWI1 (4, 7), mounted on stages (3, 6), one can move horizontally and the other can move vertically. The horizontal stepper motor is attached to the vertical stepper motor, making it possible to move to any position in the plane, the vertical stepper motor is attached to a solid stage which is mounted on an optical table from Opta (18). The stepper motors are controlled using

a RaspberryPi and two CaDPiPE boards (17) [9], the position is measured using a sliding resistor of $5k\Omega$ (5, 8). The stepper motors enable accurate movement, a more detailed description will be given in section 3.1.1. The stepper motors are powered and controlled with the practicum power unit and the signal conditioning unit (16). Attached to the stepper motor is a frame (9) to hold a very thin wire with a bead (10), made of barium titanate(IV), glued to it. The wire will be positioned through the cavity, the bead will change the frequency of the electric field depending on its position inside the cavity and the electric field strength at that position. The response of the cavity will be measured using a network analyzer, Keysight E5063A (13). This device generates microwaves which are guided into the cavity using an antenna, the device then measures the reflection using the same antenna for the frequencies in its range. The total range of the device is from 1GHz to 7GHz. A range can be set by either giving a peakcenter and a peakspan or by giving the first and last value. Also the amount of measurement points inside the range can be set. It is possible to measure different segments at the same time, this will be used later while measuring. With the use of MATLAB scripts the data can be saved and analysed. The network analyzer is connected to the cavity using a Silverline SLU18-SMNM-01.00M cable (12). Temperature changes can cause frequency shifts in the same order of magnitude as the bead, a temperature change of 1K shifts the frequency by 40-100kHz depending on the original frequency. Therefore the temperature is measured and taken into account, using a precalibrated temperature sensor (11, 15) and an Agilent 34410A 6½ digital multimeter (14).

The temperature sensor is calibrated according to the following equation

$$V = (0.0868 \pm 0.0008)T + (0.31 \pm 0.03). \quad (3.1)$$

Since only the temperature difference is of interest the equation can be rewritten to

$$\Delta T = \frac{1}{0.0868 \pm 0.0008} \Delta V. \quad (3.2)$$

In the appendix A is a graph of the original measurements and fit of the temperature and voltage dependence. Each measured frequency, $f_{measured}$, is corrected for the temperature difference, $f_{corrected}$, according to

$$f_{corrected} = \frac{f_{measured}}{1 - \alpha_{aluminium} \cdot \Delta T}, \quad (3.3)$$

with $\alpha_{aluminium}$ the thermal expansion coefficient of aluminium, $\alpha_{aluminium} = 20 \cdot 10^{-6} \text{C}^{-1}$. The ΔT is taken with respect to a zero measurement.

Using python scripts and MATLAB scripts the setup can be controlled, see sections 3.1.1 and 3.1.2.

3.1.1 Stepper motor movement

The position of the stepper motor is determined using a sliding resistor of $5k\Omega$. A voltage of 4V is applied to the resistor with a digital to analog convertor (DAC) and using an analog to digital convertor (ADC) the returning voltage can be measured, depending on the position of the stage the ADC read a certain voltage. It might be expected that a voltage of 0V gives the outermost position and a voltage of 4V the other outermost position, however this is not the case, see $V_{measured}$ in figure 3.4. Therefore the motor has to be calibrated. This is done by taking the voltages at the ends of the stages and giving that a linear relation with respect to the relative position, see $V_{relative}$ in figure 3.4. With the value 0 the outermost value and 1 the other outermost value. Knowing the total length of both stages it is possible to calculate the absolute position knowing the relative position. The horizontal stage can be moved over a total length of 135mm and the vertical stage over a length of 295mm. A more detailed explanation is available in the CaDPiPE syllabus [9].

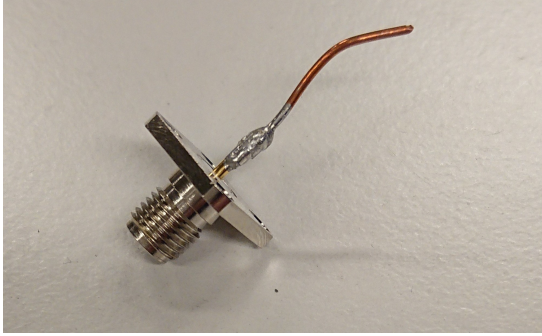


Figure 3.2: Photo of the used antenna.

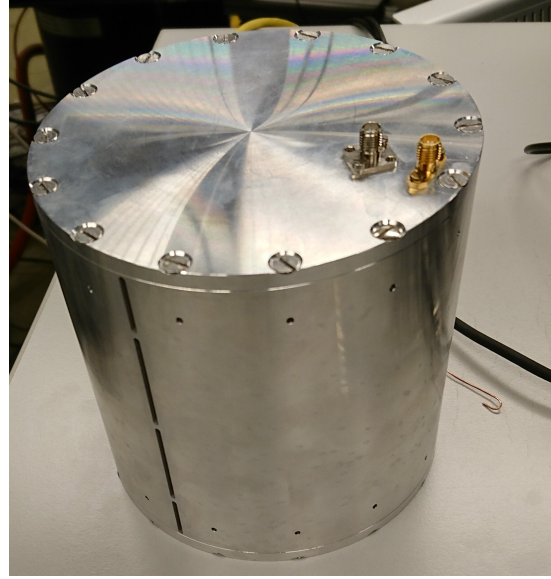


Figure 3.3: Photo of the cylindrical cavity.

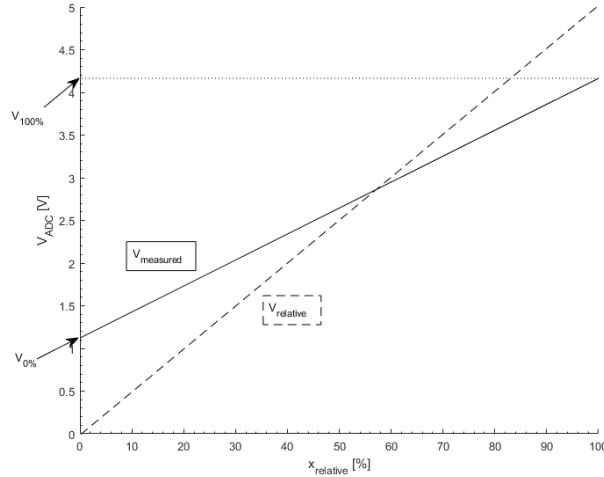


Figure 3.4: Linear relation between position and the ADC voltage measured.

3.1.2 Matlab script

The setup is automated using a MATLAB script, this script can be found in appendix C. The script makes it possible to measure one slit. The x variable is used to give a position to the horizontal stepper motor and the y is used for the vertical stepper motor. **PosStartx** is defined as the position where the bead is just inside the cavity, **PosEndx** is the position where the bead is just inside the cavity but on the opposing side, **StepSizex** is the distance the bead will move in the x direction with every step. Similar to the x coordinate, **PosStarty** is the starting position in the y direction, **PosEndy** the end position and **StepSizy** the distance the bead will move in the y direction per step. **PosOutLeftx** and **PosOutRightx** are the position where the bead is positioned outside the cavity for a zero measurement on the left and right side respectively. **PosConnectx** and **PosConnecty** are the coordinates where the bead can be connected. These eight variable will determine the bead pattern as described in the next section. At each position a measurement has to be done, to do this measurement the devices have to be connected using a usb cable to a computer or laptop, the MATLAB script **ConnectToDevices** makes a digital connection. The measurement is performed using the script **MCRSMMeasurement**, this script needs five variables to work, **peakCenters** is an array with the frequencies that want to be measured,

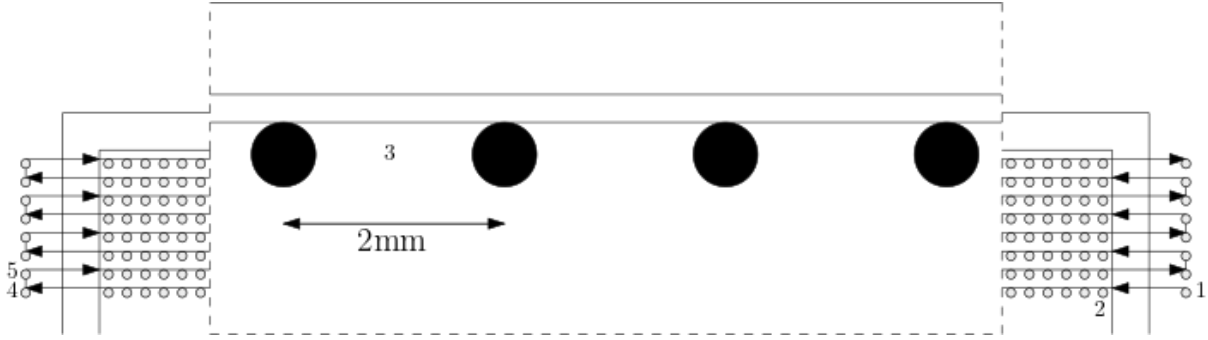


Figure 3.5: The pattern that the bead will follow during the measurement of one slit, each circle represents the position of the bead during a single MCRS measurement.

peakSpans, also an array, gives the width of the measurements corresponding to the **peakCenters**, **numPoints** are the number of points that are measured per peakcenter, the **x** and **z** are used for saving the position, x for the horizontal position and z for the vertical position, these variables are automatically changed in the script. A measurement is saved in a folder named 'peakCenters - peakSpans - time - numPoints - location', this folder contains two files rawData.mat containing the MCRS measurement and temperature.mat containing the temperature information. Before running the program it is necessary to enter the right values, all positions have to be a value between 0 and 1. When running the script it will move to the position where the bead can be attached, here the program will pause until a value is given in the command window. What happens next will be explained in section 3.1.3. This script can be used for different types and sizes of cavities, in further researches.

3.1.3 Cavity design and Bead pattern

The cavity has a specific design, in figure 3.3 an image of the cavity is shown. The cavity has 4 slits on two opposing sides, the slits have a length of 19 ± 0.05 and 36 ± 0.05 mm and a width of 2 ± 0.05 mm, the smaller slits are the ones at the top and the bottom, the larger slits are the two in the middle. The slit at the top is called slit 1 and moving down the number will increase to slit 4 at the bottom. At the top are two SMA-connectors, the one closest to the edge is used to apply RF signal to the cavity the other one is attached to the antenna. A thin wire with the attached bead will be guided through two slits of the same height, the effect of the thin wire is neglected. The stepper motors will then move the bead through the cavity. The bead will move in a specific pattern through the cavity, in figure 3.5 the pattern is visualised. First the bead is attached and moved to a position just outside the cavity on the right (1), here the first measurement is done. After that the bead will be positioned at the inside wall (2), starting here the bead will move 2.0mm to the left (3) after each measurement until it reaches the opposing wall of the cavity. It will then move out of the cavity for another measurement(4), after this measurement it will move up by 2.0mm (5) and back into the cavity and will do measurements for each 2.0mm. This will continue until the maximum height is reached. The process is repeated for the 4 different slits. This gives a total of 57 measurements per height. For the small slit there are 8 different heights measured, for the larger slit 17 measurements are done. The bead is designed to be round, however since it is self made it will not be perfect, it has a diameter of 1.5 ± 0.2 mm.

3.2 Frequencies

The full range response (2GHz to 6GHz) of the cavity can be seen in figure 3.6. The first two deep peaks at 2.22GHz and 2.466GHz are relatively close to the calculated frequencies of respectively the TM010 and TM011 modes. The theoretical frequencies that were obtained using equation 2.5 are put in a table in appendix B. Looking in this table we see a frequency of 2.186GHz for TM010 and 2.529GHz for TM011. Again the TM01 p modes are preferred. Looking for isolated strong peaks and TM01 p modes 3 more

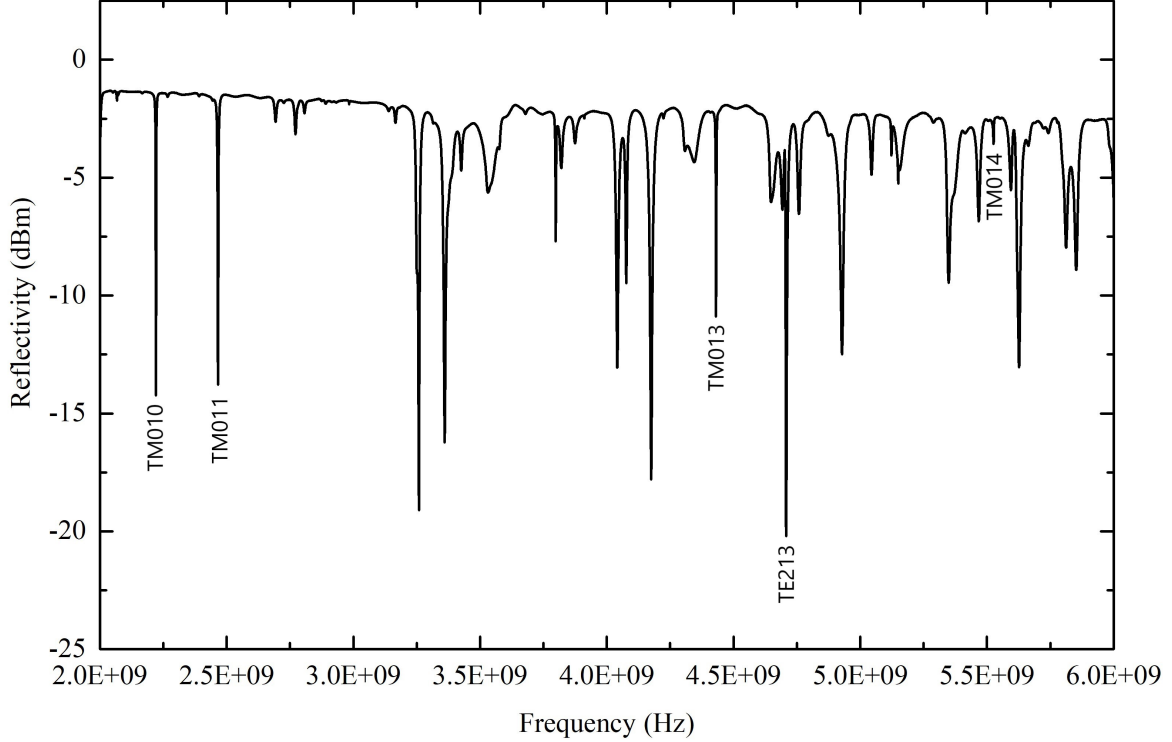


Figure 3.6: Measured response of the cavity for the frequency range from 2GHz to 6GHz. The reflectivity is measured in decibels and the frequency in Hertz. This image is made using the antenna from figure 3.2.

modes are identified and used for later measurements. The TM013 is calculated to be around 4.40GHz, a peak is observed around 4.43GHz, it is reasonable to assume this is the TM013 peak, since no other mode has a calculated frequency close to this frequency. Next is taken the strongest peak in the graph with a frequency of 4.707GHz, the closest mode is the TE213 mode, this one has a theoretical frequency of 4.717GHz. The last one taken is the small peak observed around 5.526GHz, this most likely matches the TM014 mode, 5.53GHz. Each mode is measured with a peakspan of 25MHz and 1901 points. The responses of these 5 modes are plotted in figure 3.7. In the plots it can be seen that the signal for the TM010, TM011, TM013 and TE213 are relatively strong compared to the TM014. It can therefore be expected that the results for the TM014 mode will have more noise and the results will therefore have a higher uncertainty than the four other modes. The TE213 is close to a different mode but the signal is strong enough. The signals of the TM010, TM011 and TM013 are 9-14dBm. The signal of the TE213 is stronger, 20dBm. As said the signal of the TM014 is very weak, it measures only 1.3dBm, and it is very noisy.

3.2.1 Fitting

The responses of each mode are fitted to a Lorentzian

$$L_{fit}(f; f_0, Q_0, A, a_0, a_1) = A \frac{\left(\frac{f_0}{2Q_0}\right)^2}{(f - f_0)^2 + \left(\frac{f_0}{2Q_0}\right)^2} + a_0 + a_1(f - f_0), \quad (3.4)$$

with f_0 the resonance frequency, Q_0 the Q -factor of the cavity for the specific mode. A , a_0 and a_1 are scaling factors [10].

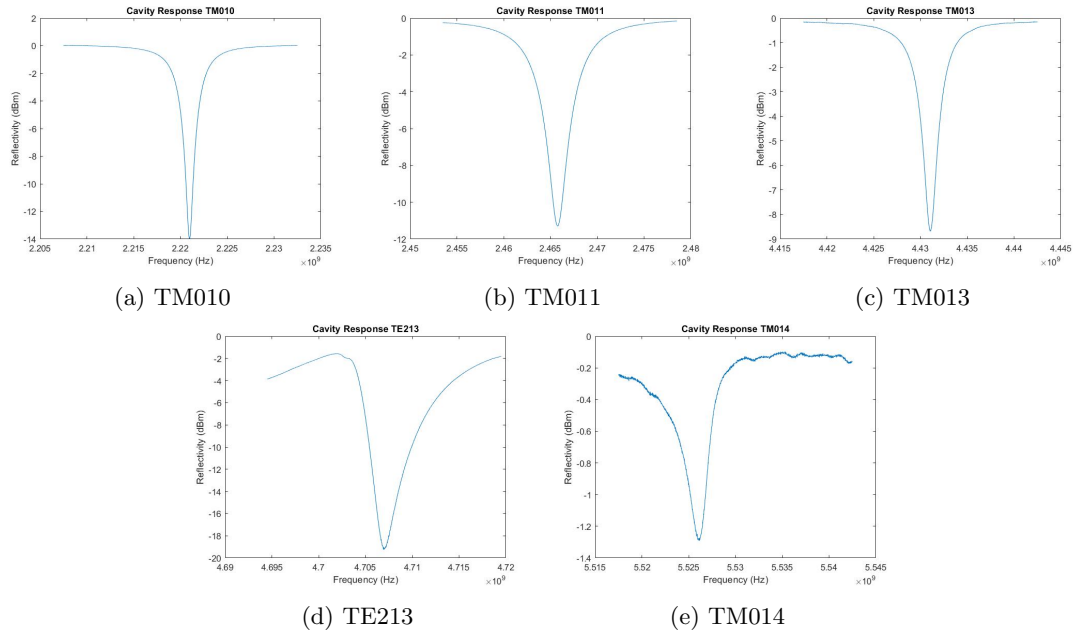


Figure 3.7: Cavity response for the 5 different modes.

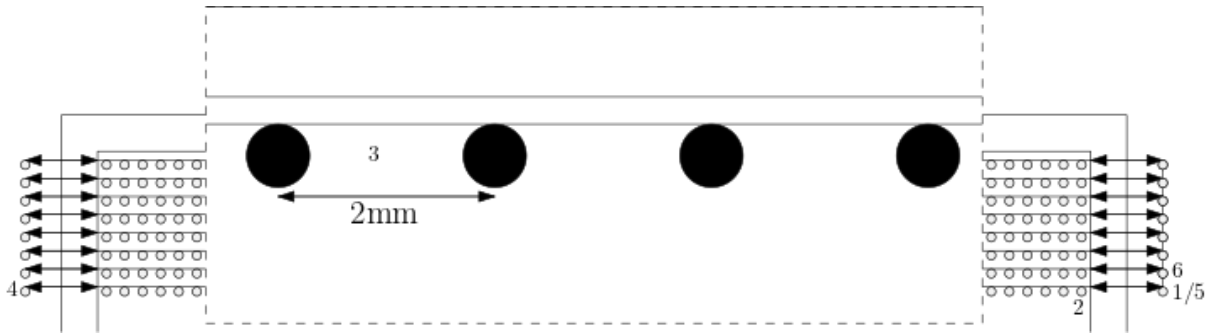
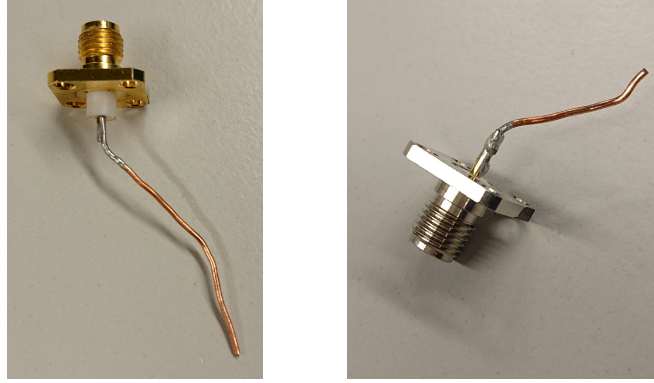


Figure 3.8: The pattern that the bead will follow during the new measurements of one slit, each circle represents the position of the bead during a single MCRS measurement.

All measurements from section 3.1.3 are fitted to the Lorentzian as given in equation 3.4. The f_0 's are put in a vector and compared to the f_0 of the measurement outside the cavity. This will give a Δf vector. This can be done for each height, giving a matrix of Δf for each position. The shift in frequency has an uncertainty of $\pm 1\text{kHz}$. This matrix can be plotted, either using a surf plot or a contour plot. Next to the Δf also the Q -factor can be obtained from the fit for each position and each mode. The same thing as with the Δf can be done for the Q -factor, this gives the Q -factor for each position inside the cavity.

3.3 One side movement

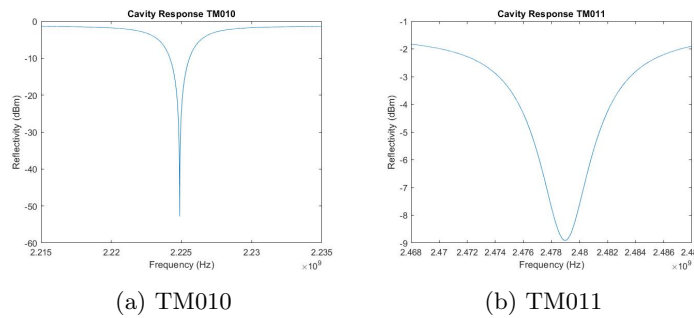
Reading out the position of the stage of the stepper motor seems to be not fast enough, as a consequence the stage looks like it overshoots the desired location, this can for example be seen in figure 4.2a by a small zigzag pattern. To check this the bead pattern is changed for an additional measurement set of the 3rd slit. Instead of measuring from the right to the left and then back from the left to the right, the measurements will only be done when moving from the right to the left, see figure 3.8, after reaching the outermost position (4) on the left it will move back to the right without doing a measurement inside the cavity (5) and move up there (6).



(a) Antenna 2

(b) Antenna 3

Figure 3.9: Antennas 2 and 3



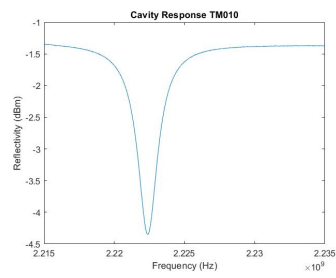
(a) TM010

(b) TM011

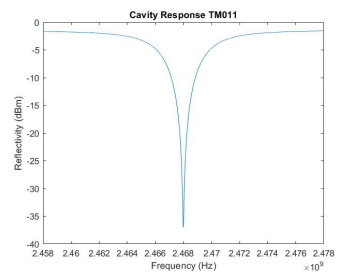
Figure 3.10: Cavity response for antenna 2 for the two modes.

3.4 Improvement signal

Since the current antenna is not specified for a specific mode the response of each mode is relatively low. To improve the signal of a single mode it is possible to design an antenna that can better excite that one specific mode. This would influence the Q -factor of that specific mode, since it will induce a deeper peak than before, this response can be narrower or wider. This would also induce a more accurate fit and therefore a more accurate field pattern. At the same time the other modes will most likely become less clear. Two more antennas are made, one to excite the TM010 and the other to excite the TM011. The antenna that excites the TM010 is named antenna 2, see figure 3.9a, and the one exciting TM011 is named antenna 3, see figure 3.9b. Using antenna 2 the full cavity is measured again for the two modes, TM010 and TM011, to view the difference of the pattern and the Q -factor. Antenna 3 is used to also measure the TM010 and TM011 modes but it will also be combined with the pattern of section 3.3. The responses of the cavity for the two modes and the two antennas can be seen in figures 3.10 and 3.11. Antenna 2 excites the TM010 to a depth of over 50dBm but the TM011 to only a depth of 9dBm, the peaks can be found at 2.225GHz and 2.479GHz. Antenna 3 excites the TM010 to over 35dBm and the TM011 to just over 4dBm, the peaks are found at 2.222GHz and 2.468GHz. The antenna design is of influence on the resonance frequency, antenna 2 is the longer antenna and can therefore influence the cavity more.



(a) TM010



(b) TM011

Figure 3.11: Cavity response for antenna 3 for the two modes.

Chapter 4

Results and Discussion

In this chapter the results will be presented and discussed. Also the uncertainty of the measurements will be taken into account and the improvement measurements will be presented. At last a discussion is given on the overall measurements and suggestions will be given to improve the measurements for future researches.

4.1 TM010

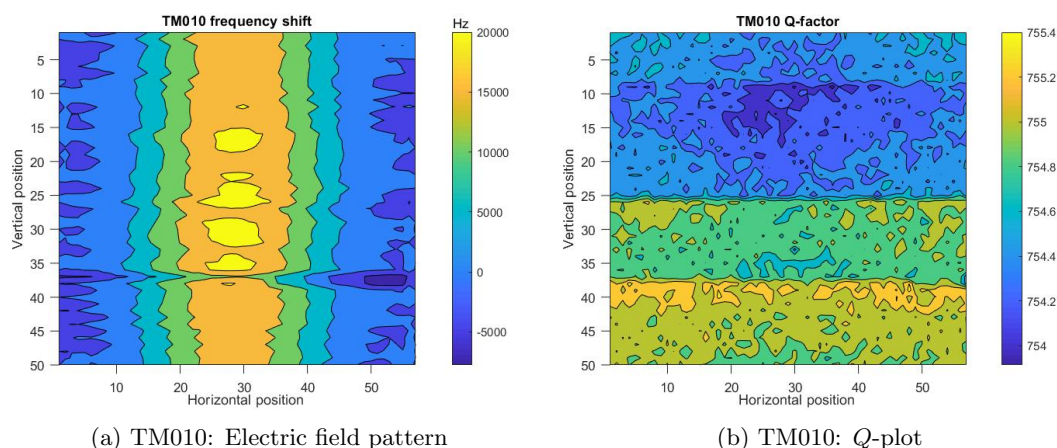


Figure 4.1: TM010

All positions are given in measurement points, the left corresponds to left side of the cavity with the antenna on the far side, the top of the graph corresponds to the side with the antenna. The frequency changes up to (20 ± 1) kHz, and has a Q -factor of 754 to 755.4 throughout the cavity. It can be seen in the graph that it is almost constant in the z direction, but not completely. Also it can be seen there is a discrepancy in the measurements, there should not be points where $\Delta f < 0$, however this is the case in this graph. The Q -plot shows straight horizontal lines at the half of the height which can be explained by the fact that this is the point where the bead has been reattached in another slit. The Q -factor decreases as the bead is positioned in a higher position.

4.2 TM011

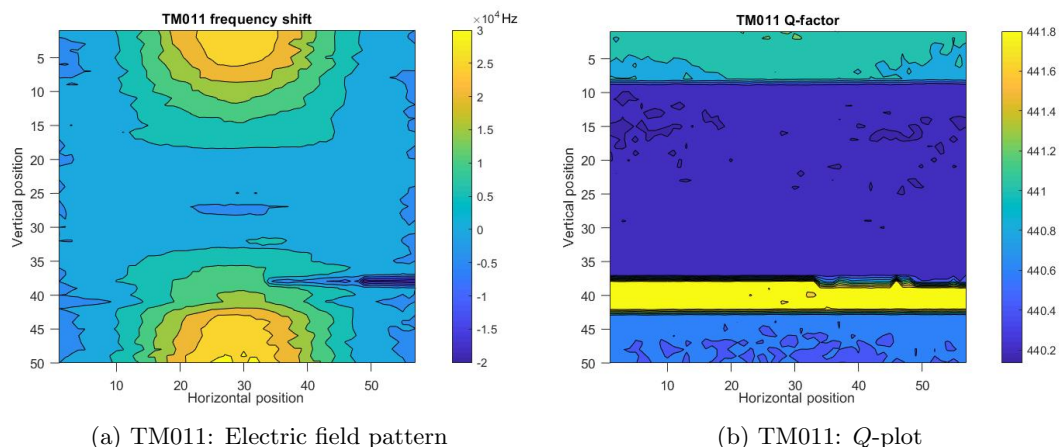


Figure 4.2: TM011

There are frequency changes up to (30 ± 1) kHz observed. The Q -factor is 440 at the center and 441 to 441.5 near the top and bottom. The two nodes in the center top and bottom are clearly visible. Also here there is a discrepancy in the measurements, at roughly the same height as in the TM010 mode $\Delta f < 0$. There is a clear minimum in the center at half of the height. The Q -plot shows rapid horizontal changes in the Q -factor, the ones at the top and bottom can be explained because the bead was moved to another slit at this point. The increase between 35 and 40 is not explainable.

4.3 TM013

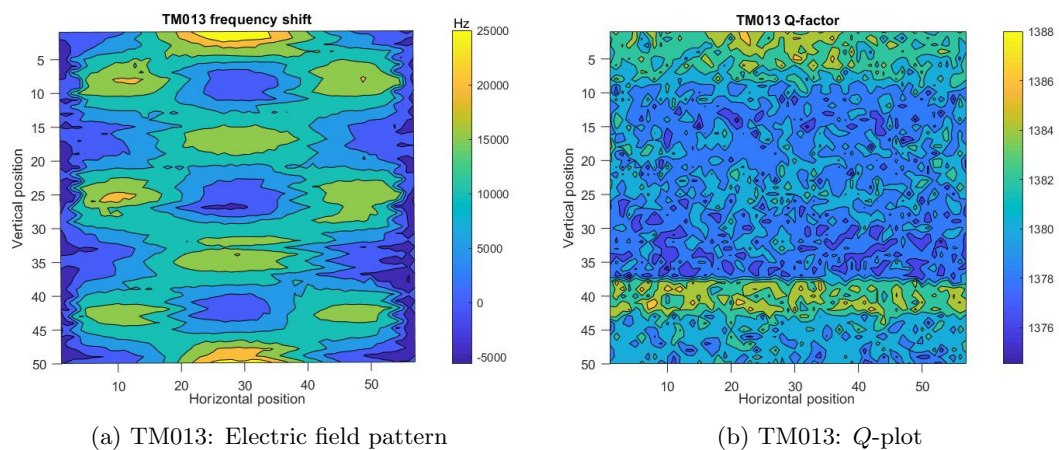


Figure 4.3: TM013

This mode shows frequency changes up to (25 ± 1) kHz. A Q -factor of 1376 to 1388 is observed. The graph is clear, showing three nodes near the outer walls and four around $r = 0$. The nodes at the top and bottom around $r = 0$ have the highest intensity. The Q -factor plot looks noisy however an increase in the Q -factor is visible near the bottom and top. The same increase in Q -factor between 40 and 45 is observed as in the TM011 mode.

4.4 TE213

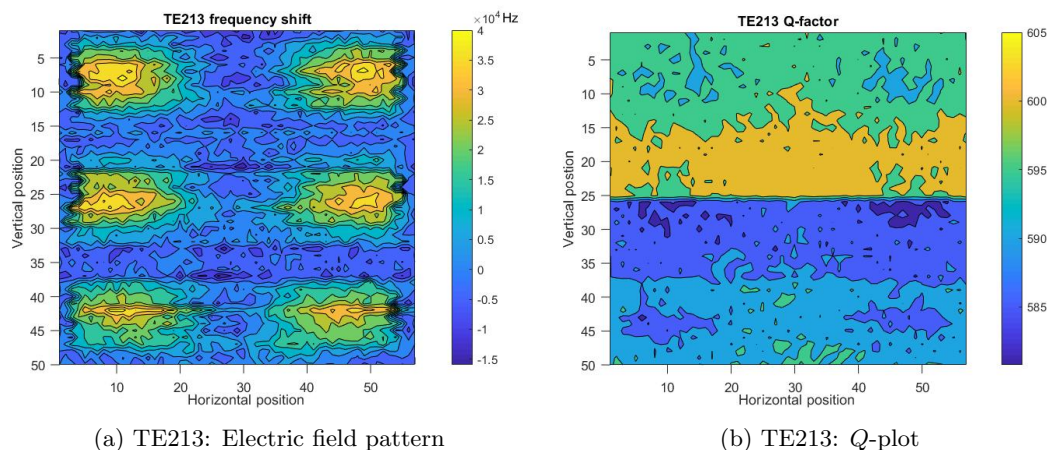


Figure 4.4: TE213

The frequency changes up to (40 ± 1) kHz. The Q -factor is 585 to 605. The electric field pattern is noisy but still showing a distinct pattern. Three ellipses are showing on both sides near the wall. The Q -factor is the highest in slit 2 and the lowest in slit 3. With a little creativity the six high intensity electric field regions are also visible in the Q -plot, as regions with a lower Q -factor than their surroundings. The Q -factor decreases as it gets closer to the top and increases as it gets closer to the bottom.

4.5 TM014

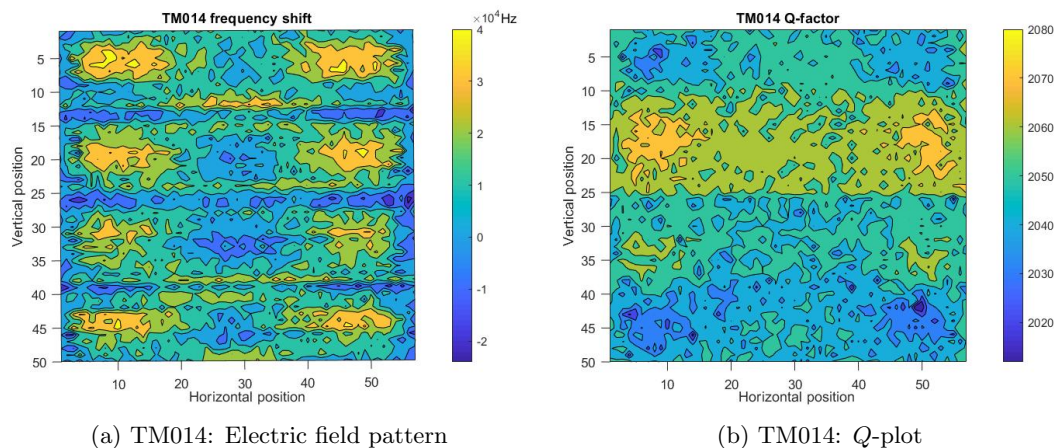


Figure 4.5: TM014

The frequency changes up to (40 ± 1) kHz. The Q -factor is ranging from 2020 to 2080. Lots of noise is observed. The four nodes close to the wall can clearly be seen, the nodes at the center axis are not so clear. The signal was not high so the effect of noise was expected. In the Q -plot one can see the four nodes from the electric field back as either an increase (middle two) or a decrease (top and bottom) of the Q -factor. The Q -factor decreases from the center to the top and bottom.

4.6 One sided movement

To look for a way to solve the zigzag pattern, the 3rd slit was measured again in the way described in section 3.3

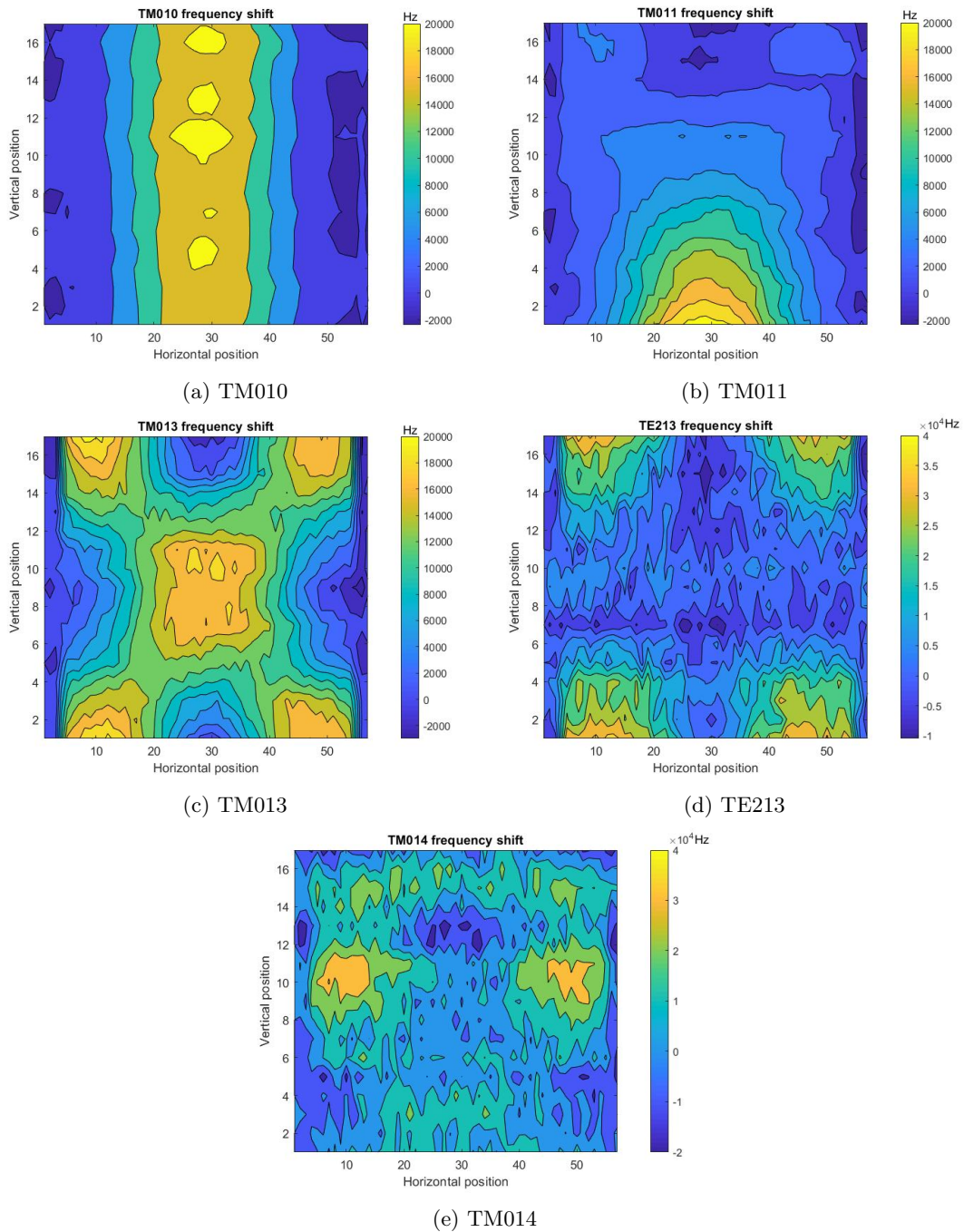


Figure 4.6: Electric field pattern of the third slit for the five different modes, using the measurement pattern as describe in 3.3. The graphs are not to scale.

It can be seen that the graphs do not have the zigzag pattern as much as before. Next to that the same characteristics are observed as before. The general pattern of the modes has stayed the same.

4.7 Improvement antenna

4.7.1 Antenna 2

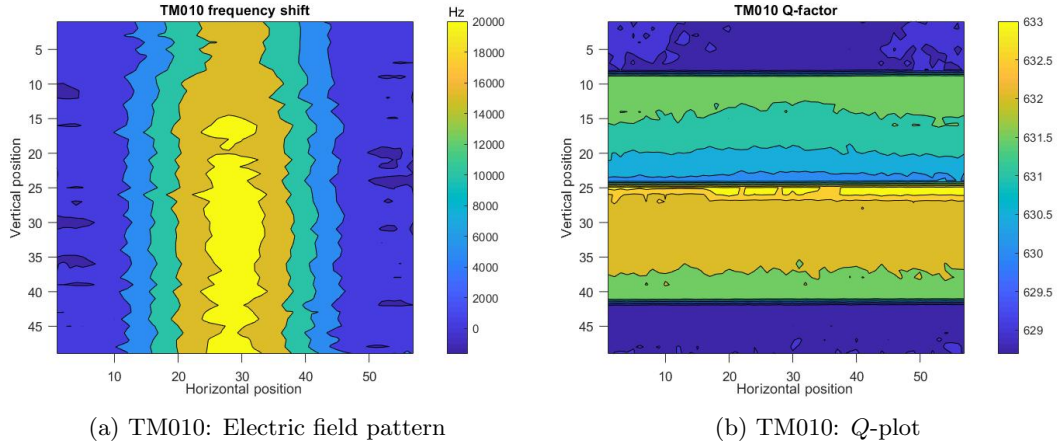


Figure 4.7: TM010 antenna 2

The electric field pattern looks to be less dependent on the z -coordinate except for the region near the top. The maximum frequency shift has not changed, it is still (20 ± 1) kHz. The Q -factor of the TM010 mode has decreased with respect to the first measurement, to a value of close to 631. This would suggest that the width of the peak has increased while also the depth of the peak has increased. The difference in Q -factor for the slits 2 and 3 with respect to slits 1 and 4 can be explained because these measurements have been done on two separate days. The temperature is slightly different for the four slits, the average temperature during the measurements of slit 2 and 3 were respectively 23.2 and 23.6°C. The slits 1 and 4 have been measured the following day, during these measurements the average temperatures were respectively 23.1 and 23.4°C. The value of the Q -factor increases within the slits 2 and 3 as the bead moves upward.

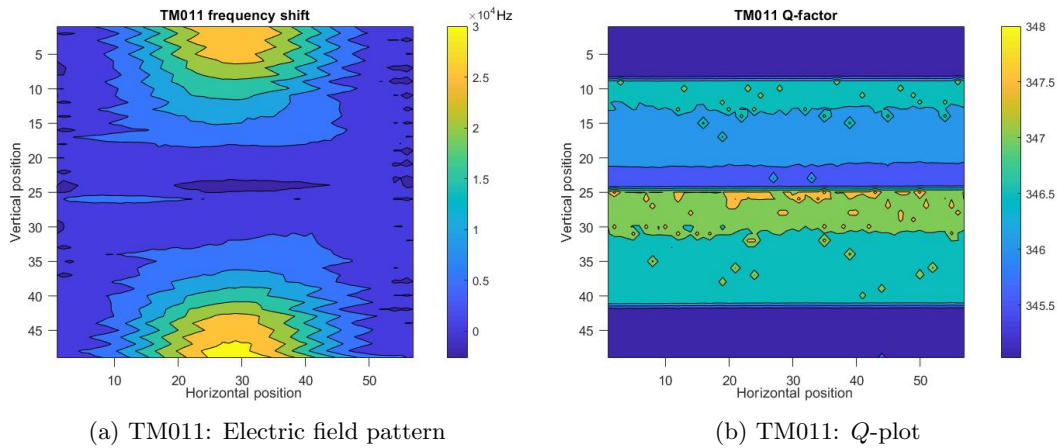


Figure 4.8: TM011 antenna 2

The pattern of the electric field looks like the one in figure 4.2a. However a zigzag pattern is clearly visible, this can be reduced by doing a different measuring pattern as described in section 3.3. The signal of this mode is 2 dBm lower than the one in the first measurement this also results in a lower Q -factor, the Q -factor has decreased from 439 to 347. The difference in Q -factor for the slits 2 and 3 with respect

to slits 1 and 4 can again be explained by the fact that the measurements have been done on two separate days. The value of the Q -factor increases within the slits 2 and 3 as the bead moves upward.

4.7.2 Antenna 3

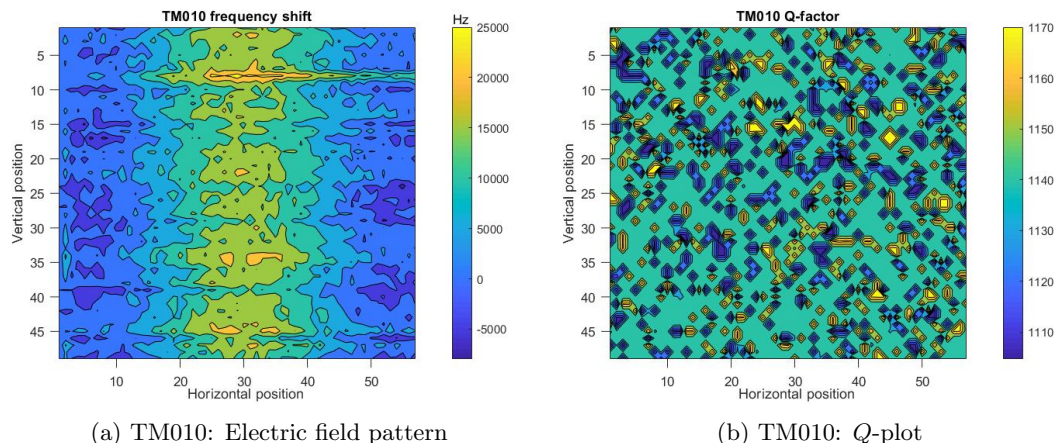


Figure 4.9: TM010 antenna 3

The signal of the response for this mode with this specific antenna is very low (4dBm), this will explain the amount of noise in the electric field pattern that is measured. The field pattern looks roughly like the two previous ones. The Q -factor has been increased even though the signal has substantially been decreased. The new Q -factor has a value between 1110 and 1170. The pattern of the Q -factor looks very different from all other Q -factor patterns. One possible explanation for this can be the low signal response.

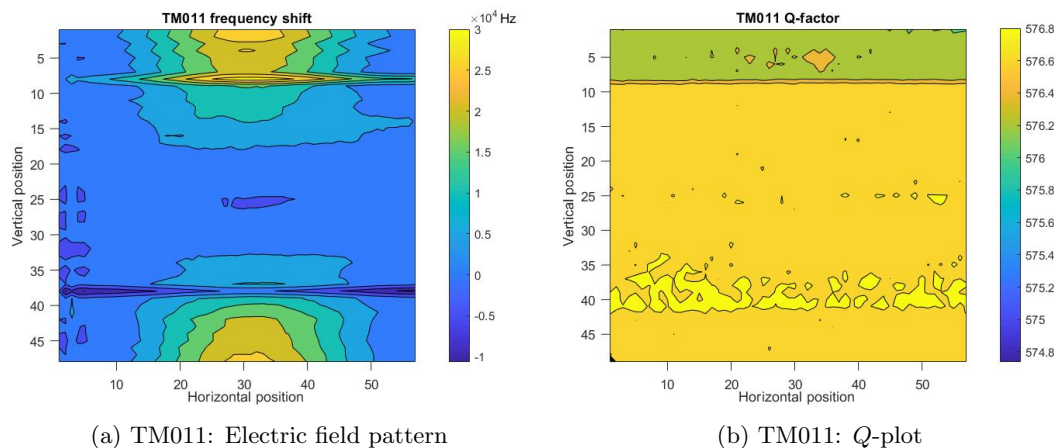


Figure 4.10: TM011 antenna 3

The electric field pattern of the TM011 mode looks similar to the one in figure 4.2a, however it does have two regions with unexpected results, this can be the result of the specific antenna design or it can be caused by a faulty reference measurement. The Q -factor has increased to a value of 576. The decrease in Q -factor for the upper slit can be explained because this measurement was done on a different day.

4.8 Discussion

The measurements can be improved in different ways. The one sided movement seems to have a large effect of reducing the zigzag pattern. Also the relatively large changes in Q -factor can be reduced by measuring the cavity on only one day, which is possible. A large cavity response gives a clear pattern. The tension inside the wire can be of effect to the Q -factor, since even though the measurements were done on the same day a difference in Q -factor is still observed for the different slits. The signal of the TM010 mode for antenna 2 is very sensitive to vibrations because of the high signal response, it is not known how this effects the measurements. A second set of measurements can be done to see whether or not the odd measurements are the result of the antenna or if they were a faulty measurement. The responses are corrected for temperature changes. The Q -factor does change over the course of time, the temperature might be of small influence but it is not the main reason. Different reasons can be a change in humidity, changing the permittivity of the air inside the cavity or a possible different pressure inside the room. The response of the TE213 mode is relatively close to another response, the accuracy of the fit might benefit from reducing the width where the network analyzer measures for this mode, currently the width is 25MHz.

Chapter 5

Conclusion

In this chapter the results will be compared to the theory. Based on the the comparison a conclusion will be made.

First the three different measurements of the TM010 mode will be compared to the theoretical field pattern of this mode given in 2.3a. The theoretical prediction clearly shows that this mode does not have any z dependence, however the experimentally obtained patterns show a z dependence. The mode has a relatively low Q -factor, this can explain why the mode is not 'perfect'. Another explanation might be the fact that there is a relatively high resistance present in the cavity around the corners, what can result in lower electric fields in this regions.

The TM011 shows roughly two semi-circles, one at the top and one at the bottom. The experimentally determined patterns also show these two semi-circles, however all measurements done on this mode do have a certain discrepancy, for the first measurement there is a region with a negative shift, for the measurements with antenna 2 there is a very clear zigzag pattern visible and for the measurements with antenna 3 there are two regions which deviate from the rest. The most reasonable explanation is that the measurement outside the cavity has gone wrong for some reason.

Following with the TM013 mode, which has according to the theory three maxima on each side near $r = R$, this is also observed in the experimentally obtained pattern. Also it is supposed to have four maxima at $r = 0$, which are just below the intensity of the ones near $r = R$. The experimentally obtained pattern does show the four maxima, however the intensities of the one at the top and the one at the bottom are higher than the ones around $r = R$. There is no current present in the slits, but only next to the slits. This can result in lower intensities around the slits, while at the bottom and top the current is free to move and thus creating a higher intensity.

The TM014 should show four maxima of high intensity close to $r = R$ and five of lesser intensity at $r = 0$. The experimentally obtained pattern is noisy, however the four maxima close to $r = R$ can be observed. The maxima of lesser intensity at $r = 0$ are barely visible, most likely this is because of the antenna could not excite this mode good enough, which resulted in a low cavity response.

Lastly the TE213 is showing three ellipses close to $r = R$. This is also observed in the experimental pattern, however the experimental pattern does look a little noisy, this can be explained because the peak in figure 3.7d is very wide resulting in a lower Q -factor and it has a neighbouring peak which might influence the accuracy of the fit.

As was said in section 4.8 the measurements can be improved, either by improving the read out of the position of the stage by the ADC or by doing multiple measurements for each mode. Also doing the measurements on one day can have an effect on the the accuracy of the Q -factor distribution. The difference of the Q -factor is not yet explainable, a possible further research can look into the origin of this, it can be concluded that the temperature is not of large importance for the Q -factor.

Antenna 2 lowers the Q -factor for both the TM010 and the TM011 modes, antenna 3 on the other hand increases the Q -factor for both modes. Therefore it can be concluded that next to the design of the cavity also the design of the antenna is of importance for the Q -factor.

Referring back to the research question in chapter 1: what is the electric field profile within an inverse cylindrical cavity for different resonance frequencies? It is possible to answer this question. The theoretical electric field patterns is in general the same as the experimentally determined patterns, with the exception of a small differences in intensity for the TM013 mode and the noise in the TM014 and TE213 modes. The experimental frequencies do differ from the theoretical value, this can be explained by the fact that the cavity is not ideal and the electric field will therefore penetrate the wall of the cavity, making the cavity slightly bigger.

TM modes should be suppressed by the design of the cavity. Displacement currents \mathbf{K} will move from the top to the bottom and vice versa, since the cavity exist of three separate components in this direction, the top plate, curved wall and bottom plate, a high resistance is present, which will suppress the TM modes, especially the TM010 and TM011 modes. However the modes are pretty clearly observed, which suggests that the resistance is not high enough.

Using the result of this study it is now possible to obtain the electron density distribution inside the cavity when a plasma is created. The setup that is used can be reused to do the same procedure for a different cavity.

Bibliography

- [1] L. G. Hector and H. L. Schultz. “The Dielectric Constant of Air at Radiofrequencies”. In: *Physics* 7.4 (1936), pp. 133–136. DOI: 10.1063/1.1745374.
- [2] I.H.Hutchinson. *Introduction to Plasma Physics*. 2001. URL: http://silas.psf.mit.edu/introplasma/chap1.html#tth_sEc1.1.
- [3] MAILADIL T. SEBASTIAN. “CHAPTER TWO - MEASUREMENT OF MICROWAVE DIELECTRIC PROPERTIES AND FACTORS AFFECTING THEM”. In: *Dielectric Materials for Wireless Communication*. Ed. by MAILADIL T. SEBASTIAN. Amsterdam: Elsevier, 2008, pp. 11–47. ISBN: 978-0-08-045330-9. DOI: <https://doi.org/10.1016/B978-0-08-045330-9.00002-9>. URL: <http://www.sciencedirect.com/science/article/pii/B9780080453309000029>.
- [4] A. Piel. *Plasma Physics: An Introduction to Laboratory, Space and Fusion Plasmas*. Springer, 2010. ISBN: 978-3-642-10491-6.
- [5] M.C.N. Fiolhais et al. “MAGNETIC FIELD AND CURRENT ARE ZERO INSIDE IDEAL CONDUCTORS”. In: *Progress In Electromagnetics Research B* (2011), pp. 187–212. URL: <http://www.jpier.org/PIERB/pierb27/10.10082701.pdf>.
- [6] Ferdi van de Wetering. “Formation and dynamics of nanoparticles in plasmas”. English. Proefschrift. PhD thesis. Department of Applied Physics, Feb. 2016. ISBN: 978-90-386-4018-1. DOI: 10.6100/f3331ca8-0d98-4cf4-92cb-58a6a8ca047c.
- [7] *Introduction to Electrodynamics*. ISBN 978-1-108-42041-9. Cambridge University Press, 2018.
- [8] B W Feng et al. “Size and electron density of open-air plasmas diagnosed by optical imaging”. In: *Journal of Physics D: Applied Physics* 52.26 (Apr. 2019), p. 265203. DOI: 10.1088/1361-6463/ab15cc. URL: <https://doi.org/10.1088/1361-6463/ab15cc>.
- [9] Sander Nijdam and Hjalmar Mulders. *Control and Data Processing in Physics Experiments*. 2019.
- [10] Marc van der Schans et al. “Decay of the electron density and the electron collision frequency between successive discharges of a pulsed plasma jet in N₂”. In: *Plasma Sources Sci. Technol.* 28.3 (2019), p. 14. URL: <http://stacks.iop.org/0963-0252/21/i=3/a=034005>.
- [11] Plasma Universe. *Quasi-neutrality*. 2019. URL: <https://www.plasma-universe.com/quasi-neutrality/>.
- [12] *Wolfram Mathematica*. Internet page. Version 12.0. Wolfram, 2019. URL: <http://www.wolfram.com/mathematica/?source=nav>.

Appendix A

Temperature sensor calibration

The temperature sensor that has been used in this study has been calibrated from 23°C to 35°C. This calibration is performed by setting an accurate temperature and measuring the voltage output. 250 voltage measurements are done for each temperature. The average value with the standard deviation is given. A linear fit is performed through the measurements with their uncertainty, see figure A.1.

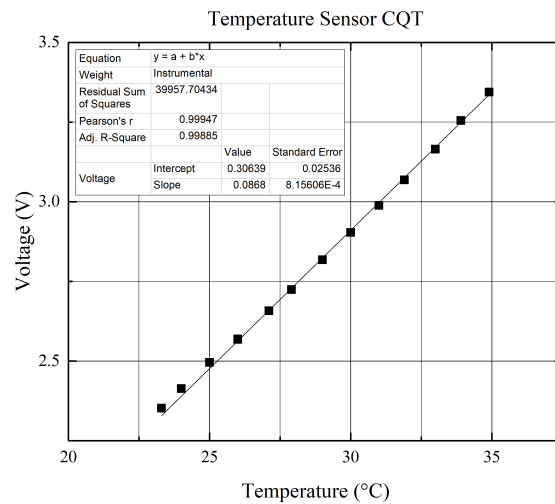


Figure A.1: Calibration of the used temperature sensor, done by I. Bolk.

Appendix B

Frequency table

Table B.1: Frequencies of each mode as calculated using equation 2.5

Mode	f (GHz)	Mode	f (GHz)	Mode	f (GHz)	Mode	f (GHz)
TE110	1.67369	TE120	4.84637	TE123	6.16689	TM024	7.14379
TE111	2.10171	TE411	4.99809	TE221	6.22713	TE223	7.19059
TM010	2.18604	TE121	5.01031	TM023	6.30257	TM115	7.24775
TM011	2.52878	TM020	5.01788	TM312	6.33249	TE015	7.24775
TE210	2.77634	TM113	5.16481	TE314	6.35919	TE320	7.28601
TE112	3.04383	TE013	5.16481	TE512	6.36201	TM412	7.35159
TE211	3.05352	TM021	5.1764	TM120	6.37734	TE321	7.39607
TM012	3.35298	TM212	5.31579	TE020	6.37735	TE315	7.41502
TE010	3.48311	TE114	5.35312	TM121	6.50279	TM123	7.43059
TM110	3.48311	TE313	5.39703	TE021	6.50281	TE023	7.4306
TE011	3.70782	TE412	5.46156	TE115	6.5726	TM220	7.65148
TM111	3.70783	TE122	5.47275	TE222	6.60492	TM314	7.71307
TE212	3.76454	TM014	5.53475	TM015	6.72136	TE322	7.71684
TE310	3.81899	TM022	5.62519	TM122	6.86543	TE514	7.73732
TE311	4.025	TE214	5.79333	TE022	6.86544	TM221	7.75635
TE113	4.16467	TM310	5.79972	TM410	6.89799	TE130	7.7597
TE012	4.31227	TE510	5.83193	TM214	6.9028	TE116	7.8086
TM112	4.31228	TM310	5.9374	TE215	6.93584	TE131	7.86313
TM013	4.39568	TM511	5.96887	TM313	6.94118	TM030	7.86645
TE312	4.58785	TM213	6.02804	TE513	6.96812	TM413	7.88197
TM210	4.6684	TE220	6.09601	TM411	7.01414	TM215	7.88618
TE213	4.71713	TE413	6.15697	TE414	7.01567	TM016	7.93421
TE410	4.83373	TE014	6.16333	TE124	7.02438	TE224	7.93826
TM211	4.83838	TM114	6.16334				

Appendix C

Matlab scripts

C.1 Main script

file:S:\Experimental_Data\MCRS\LowPressureRFSheathExploration\RoyClevis_RawData_InverseCavity\Scripts\MCRS_measurements\MovementBeadIncludingMeasurement.m

```
%% Run Network Analyser for MCRS measurements in horizontal-vertical plane

clc
clearvars

%% Start variables
%Define starting/end position and stepsize (x: 0 right, 1 left) (y: 0 bottom, 1 top)
PosStartx = 0.095; %horizontal position inside cavity start
PosStarty = 0.5518; %vertical start postion
StepSizeX = 0.015; %stepsize in horizontal direction
StepSizeY = 0.0068; %stepsize in vertical direction
PosEndx = 0.905; %horizontal position inside cavity end
PosEndy = 0.6606; %vertical end position
PosOutRightx = 0; %horizontal position with the bead outside the cavity on the right
PosOutLeftx = 1; %horizontal position with the bead outside the cavity on the left
PosConnectx = 0; %horizontal position for connecting the bead
PosConnecty = 0.5518; %vertical position for connecting the bead

%Connect to measurement devices
run ConnectToDevices

%Peaks of interest
peakCenters = [2.225 2.468] * 10^9;
peakSpans = [0.02 0.02] * 10^9;
numPoints = 4001;
z = 11;
x = 11;

run MCRSMeasurement
%% Moving to easy position for connecting
%Send starting position to RPi
system(sprintf('C:\\Program Files\\Putty\\plink.exe' -ssh CaDPiPE_admin@169.254.206.107 -pw Ph4$EvV1\r cd /h
system(sprintf('C:\\Program Files\\Putty\\plink.exe' -ssh CaDPiPE_admin@169.254.206.107 -pw Ph4$EvV1\r cd /h

%% Measurement loop
%Connect bead to setup here
proceed = input('Connect bead here. When ready enter 0 ');

%Movement through cavity
for y = PosStarty:2*StepSizeY:PosEndy
```

```

x = PosOutRightx; %Location for saving
z = y; %Location for saving
%Move to position out of cavity right side
system(sprintf('"C:\\Program Files\\Putty\\plink.exe" -ssh CaDPiPE_admin@169.254.206.107 -pw Ph4$EvV1\r cd /h
system(sprintf('"C:\\Program Files\\Putty\\plink.exe" -ssh CaDPiPE_admin@169.254.206.107 -pw Ph4$EvV1\r co

run MCRSMMeasurement %Performing measurement

%Horizontal movement to the left
for x = PosStartx:StepSize:PosEndx

    system(sprintf('"C:\\Program Files\\Putty\\plink.exe" -ssh CaDPiPE_admin@169.254.206.107 -pw Ph4$EvV1\r cd /h
    run MCRSMMeasurement %Performing measurement

end

%Move out of cavity left side
system(sprintf('"C:\\Program Files\\Putty\\plink.exe" -ssh CaDPiPE_admin@169.254.206.107 -pw Ph4$EvV1\r cd /h
x = PosOutLeftx; %Location for saving

run MCRSMMeasurement %Performing measurement

%Define new height
y2 = y + StepSize;

if y2 > PosEndy
    %Stay at the same height and move out of the cavity right side
    system(sprintf('"C:\\Program Files\\Putty\\plink.exe" -ssh CaDPiPE_admin@169.254.206.107 -pw Ph4$EvV1\r cd /h
else
    system(sprintf('"C:\\Program Files\\Putty\\plink.exe" -ssh CaDPiPE_admin@169.254.206.107 -pw Ph4$EvV1\r cd /h
    z = y2; %Location for saving

    %Horizontal movement to the right one level heigher
    for x = PosEndx:-StepSize:PosStartx

        system(sprintf('"C:\\Program Files\\Putty\\plink.exe" -ssh CaDPiPE_admin@169.254.206.107 -pw Ph4$EvV1\r cd /h
        run MCRSMMeasurement %Performing measurement

    end

end

end

%Move out of cavity right side
system(sprintf('"C:\\Program Files\\Putty\\plink.exe" -ssh CaDPiPE_admin@169.254.206.107 -pw Ph4$EvV1\r cd /h
x = PosOutRightx;

run MCRSMMeasurement %Performing last measurement

```

C.2 Script for making the connection to the measuring devices

file:S:\Experimental_Data\MCRS\LowPressureRFSheathExploration\RoyClevis_RawData_InverseCavity\
Scripts\MCRS_measurements\ConnectToDevices.m

```

%% Connect to measuring devices
% Adapted from:
% S:\Experimental_Data\Dusty_Plasmas\2019-BartPlatierAndTimStaps\programming\matlab program for network analysis
% Run Network Analyser for MCRS measurements
% Authors: Tim Staps and Bart Platier
% Version: 0.1 2019-01-31 first version
%          0.2 2019-04-05 include temperature sensor and function
%          generator for pulsed measurements
%

```

```

% Equipment:      network analyzer      Agilent Technologies E5063A
%                temperature sensor    Agilent Technologies 34410A
%                function generator (rf) Agilent Technologies 33250A (not used in this script)
%
% Adapted by:    Roy Clevis

% Reset all instruments
instrreset

% Main data folder
date_folder = [datestr(now, 'yyyy') '-' datestr(now, 'mm') '-' datestr(now, 'dd')];
main_folder = ['S:\Experimental_Data\MCRS\LowPressureRFSheathExploration\RoyClevis_RawData_InverseCavity\Measurements'];
mkdir(main_folder)
cd(main_folder)
fprintf('Currently working in: \n%s \n\n', main_folder)

% Temperature read-out setting
tau = 1; % time period between temperature
pause_duration = 1;

%% Initialization of network analyzer

% Define connection parameters for the network analyzer
nwa_visa = 'USB0::0x0957::0x1709::MY54100616::0::INSTR'; % define instrument VISA address
nwa = visa('keysight', nwa_visa); % create a VISA connection to instrument
nwa.InputBufferSize = 10e6; % set up buffer size for data transfer
nwa.ByteOrder = 'littleEndian'; % set up order of bytes for data transfer

% Start communication with network analyzer
fopen(nwa); % open connection to the instrument
clrdevice(nwa); % clear hardware buffer of instrument
nwa_id_string = query(nwa, '*IDN?');
fprintf('Connected to: %s', nwa_id_string);

% Initialize data transfer
fprintf(nwa, ':TRIG:SOUR BUS');
fprintf(nwa, ':INIT1:CONT OFF');
fprintf(nwa, ':FORM:BORD SWAP');

%% Initialization of digital multimeter

% Define connection settings
IviInfo = instrhwinfo('ivi'); % set communication protocol to I-VI
makemid('Ag34410', 'Ag34410.mdd'); % create the MATLAB instrument driver
tps = icdevice('Ag34410.mdd', ... % create a device object
              'USB0::0x0957::0x0607::MY47003978::0::INSTR', ...
              'optionstring', 'simulate=false');

connect(tps) % open connection

% Identify device
tps_util = get(tps, 'Utility');
tps_driver_id = get(tps, 'InherentIviAttributesDriverIdentification');
tps_instr_id = get(tps, 'InherentIviAttributesInstrumentIdentification');
tps_vendor = get(tps_driver_id, 'SpecificDriverVendor');
tps_model = get(tps_instr_id, 'InstrumentModel');
fprintf('Connected to: %s, %s \n', tps_vendor, tps_model)

```

C.3 Script for making a single MCRS measurement

file:S:\Experimental_Data\MCRS\LowPressureRFSheathExploration\RoyClevis_RawData_InverseCavity\Scripts\MCRS_measurements\MCRSMMeasurement.m

```

%% Connect to measuring devices
% Adapted from:
% S:\Experimental_Data\Dusty_Plasmas\2019-BartPlatierAndTimStaps\programming\matlab program for network analysis

```

```

% Run Network Analyser for MCRS measurements
% Authors: Tim Staps and Bart Platier
% Version: 0.1      2019-01-31  first version
%          0.2      2019-04-05  include temperature sensor and function
%                               generator for pulsed measurements
% Equipment:  network analyzer      Agilent Technologies E5063A
%            temperature sensor     Agilent Technologies 34410A
%            function generator (rf) Agilent Technologies 33250A (not used in this script)
%
% Adapted by: Roy Clevis

%% mcrs measurements

% Settings for frequency sweep
numPointsSweep = nwaSweepSetup(nwa, ... % total number of sweep points for
                               numPoints, peakCenters, peakSpans);
number_of_segments = numPointsSweep/numPoints; % number of separate frequency sw

% Define data folder based on current timestamp and location
data_folder = ['peakcenter' num2str(peakCenters) '-peakspan' num2str(peakSpans) '-time' datestr(now, 'HH') 'h'
              datestr(now, 'SS') 's' '-numPoints' num2str(numPoints) '-locationx' num2str(x) '-locationy' num
mkdir(main_folder, data_folder)
cd([main_folder data_folder '\'])

% Initialize count and time
n_count = 1;
t0 = tic;

% MCRS measurement
time = toc(t0);
tps_init = get(tps, 'Measurementlowlevelmeasurement');
invoke(tps_init, 'initiate')
T = invoke(tps_init, 'fetch', 5);
t_T(n_count) = time(1);
[f, P] = readTraceNwa(nwa, numPointsSweep);
freqVector(:,1) = f(1:numPointsSweep);
dataMatrix(:,1) = P(1:numPointsSweep);
pause(pause_duration)

% Save data to raw mcrs data file
save('rawData.mat', 'time', 'freqVector', 'dataMatrix')
fprintf('MCRS data saved as: %s \n\n', [main_folder data_folder '\rawData.mat'])

% Save temperature data
save('temperature.mat', 't_T', 'T')
fprintf('Temperature data saved as: %s \n\n', [main_folder data_folder '\temperature.mat'])

cd(main_folder)

```